4. Discussion

4.1. Cr_2O_3/Cr(110)

As mentioned before, one of the main reasons we chose thin films of Cr_2O_3(0001) as templates for the epitaxial growth of Al_2O_3(0001) was the fact that the former belongs to the group of oxides that have been extensively studied. Furthermore, it is well known that Cr_2O_3 and Al_2O_3 are isomorphous. In fact, this relationship between the two oxides was exploited by Xu et al[95,96] in their work on the electronic band structure of the Cr_2O_3(111) system. Although the electronic structures of both oxides are different (most importantly d-orbitals are present only in Cr_2O_3), the electronic structure of the oxygen sub-lattices should nevertheless be comparable. This is most clearly demonstrated by the fact that the oxides differ only slightly in their lattice parameters.

There have been a few reported cases concerning the epitaxial growth of an oxide on a lattice-matched dissimilar metal substrate. The Cr_2O_3|Cr(110) system is one of the few examples[68,70,72]. Epitaxial thin films of the Cr_2O_3 system at T> 500 K are used as model systems of the Cr_2O_3(0001) surface[74,77]. Thin films of Cr_2O_3 grown on single crystal surfaces have been extensively investigated by a host of workers. The oxide formed on Cr(110) at 825 K and high O_2 exposures is the Cr_2O_3(0001)||Cr(110) with an ordered unit cell whose parameters (0.47± 0.03 nm, and 0.28 nm) correspond to well ordered oxygen positions with Cr^{3+} termination[74]. Thin films of Cr_2O_3 grown on Cu(110) at 20 L O_2 annealed to 673-773 K possessed two types of structures based on the thickness of the film. Cr^{2+} species existed only for very low coverages. At high coverages, Cr^{3+} predominates[97]. There is therefore a general consensus that the oxide film exhibits a well ordered, (111)-oriented oxide surface[95]. We therefore believe, based on the extensive and conclusive literature findings and experimental evidence, that the thin Cr_2O_3 films we used are of the Cr_2O_3(0001) type.

.

4.2 Deposition of Al at 300 K Followed by Oxygen Exposure and Annealing to High Temperatures.

We saw in figure 3.3 of section 3 that attempts to deposit metallic aluminium on the Cr_2O_3(0001) surface at 300 K followed by oxygen exposure led to an instantaneous oxidation of aluminium as revealed by the appearance of an Auger transition around 56 eV, which is due to trivalent aluminium. The long range order of the substrate was also lost. This was undesirable because we were aiming at preparing thin, well ordered films of Al_2O_3. Two possibilities may explain this behavior: i) Al extracts oxygen out of the chromia substrate, or ii) it reacts with water vapour, or oxygen radicals possibly present in the chamber ambient, before getting into contact with the surface. However, the second possibility is very unlikely, since the total pressure in the vacuum chamber did not exceed 10^{-9} mbar during Al evaporation episodes. Rather, we believe from the spectroscopic evidence that an aluminothermic reaction[98,99,100,101] could have taken place at the surface on the microscopic scale. The tendency of most metals to react with oxygen of metal oxide substrates is well known. The most relevant examples in this context are probably the reaction of Cr with ZnO surfaces[102] and the interaction of Al with PdO[103] for which XPS provided evidence for Al_2O_3 formation. We did not observe any Al Auger signal at 1386 eV, although this peak is often mentioned in the literature as one of the most intense Al Auger signals.

The phenomenon of aluminothermy was coined by Hans Goldschmidt in 1894[104]. The process facilitates the extraction from ores of metals (Fe, Cr, Mn, etc.) that cannot be easily reduced through other processes. The metal products of this reaction are carbon-free hence providing an elegant way of excluding carbide formation. The driving force of the process is the strong exothermic reaction, which in turn is a consequence of the high lattice energy of Al_2O_3 that is the end product of the process [105,106]. The classical application of this phenomenon is the thermite process, which is the reaction between Al and Fe_2O_3 used for joining huge steel parts together, eg., rail tracks[106]. The highly exothermic reaction facilitates the application of the reaction in the disposal (detonation) of unused explosives and bombs, through heating (up to 2400°C) of the bomb's outer casing[107].

4.3 Co-deposition of Al and Oxygen (AES)

In thin film preparation, co-deposition is the method of choice where the step-wise deposition methods fail. The main disadvantages of the latter have been mentioned before, namely, difficulties in oxidising the deposited metallic films and controlling the film thickness. Because epitaxy between two substances is temperature dependent (epitactic temperature) the co-deposition method also has the disadvantage that the epitactic temperature has to be established.

Over the years, the oxidation of bulk Al, thick Al films and various low index single crystal surfaces has been the subject of a number of studies using various techniques[108,109]. The initial stages of O_2 adsorption and reaction are very complex and only partly understood.

At 30 K, O_2 adsorbs dissociatively on clean Al with a sticking probability around unity[90]. This sticking coefficient becomes very low (ca. 0.01-0.05) at 300 K. It is believed that a chemisorbed, but unreacted form of oxygen may be formed by low O_2 exposures around 300 K, and that an increase in either the O_2 exposure or the temperature causes the formation of an amorphous oxide film. Evidence for the chemisorbed oxygen pre-cursor state has been reported for Al(111) but not for the (100) and (110) surfaces. In AES studies, the presence of an O(KLL) peak (510 eV) and the absence of the Al peak at 54 eV (trivalent Al) for low O_2 exposures is usually taken as proof of a chemisorbed but unreacted oxygen state[110,111]. When both peaks appear at higher O_2 exposures, a two phase adsorption process takes place. First, there is oxygen chemisorption on the Al surface and then at higher O_2 exposure, reaction between the two species occurs to form an amorphous Al_2O_3 layer. Other works reported conflicting results, both in the magnitude and direction of change[112,113]. However, photoemission studies of O_2 adsorption on Al revealed a new Al(2p) state at a binding energy 1.4 eV higher than the value for metallic Al at 72.8 eV and distinct from the trivalent Al^{3+} state at 75.5 eV which is associated with the bulk oxide[113,114]. This intermediate state is believed to arise from the chemisorbed oxygen overlayer.

Although the substrate we employed in the preparation of the thin alumina films is totally different from the Al single crystal surfaces discussed above, a thorough understanding of the interaction of Al with oxygen is still relevant. In both experiments (stepwise and co-deposition), the first Al state we observed was the one at 56 eV, which is comparable to the 54 eV state in the literature. The kinetic energy of the Auger electron is down-shifted by ~10 eV from the value observed for metallic Al (66 eV), because of charge redistribution. We assume therefore that even in the early stages of co-deposition of Al and oxygen, the oxygen species is comparable to that found in bulk oxides. This would suggest that both the temperature and oxygen exposure were high enough for this scenario to take place.

Three peaks were evident in the Auger spectra of the thin alumina films we investigated. These were the 56, 38 and 24 eV states. Wytenburg in work on Al_2O_3 on Ag(110) and Ag(111) surfaces, also identified three Al peaks, but at different energy positions at 54, 47 and 39 eV respectively. As has been mentioned, the peak at 56 eV is characteristic of both oxidised Al films and bulk Al_2O_3. Wytenburg[90] ascribed the 47 eV peak as arising from oxidised Al only and the small peak at 39 eV as due to the replacement of the Al-induced transition by a new Al_2O_3-induced transition. In our case, the peak at 38 eV did not appear at low Al_2O_3 coverages, whilst that at 24 eV was present from the onset of Al deposition. The fact that the 38 eV peak appeared at high coverages (more than 15 Å) only tends to support Wytenburg's theory that it had to be Al_2O_3-induced.

Table 4.1 Auger Peak Assignments[90]

Al-O Auger Cross-Transition Assignments				
This work	**Wytemburg**	**Hoffman et al**	**Mechanism 1**	**Mechanism 2**
56	54	55	$Al(L_{2,3})O(L_{2,3}L_{2,3},1D)$	$Al(L_{2,3})O(L_{2,3})O(L_{2,3})$
38	47	47	$Al(L_{2,3})O(L_1L_{2,3},{}^3P)$	$Al(L_{2,3})O(L_{2,3},L2_{,3},)$
24	39	39	$Al(L_{2,3})O(L_1L_{2,3},{}^1P)$	$Al(L_{2,3})O(L_{2,3})O(L_1)$

The oxygen-induced Auger peaks have been extensively studied. That they have been assigned to Al-O cross-transitions is generally accepted[90], but the actual assignment varies. The two most common assignments are presented in table 4.1.
The difference between the two mechanisms is the localisation of holes on one or two oxygen atoms. An attempt is made to interpret the observations as cross-transition because Al^{3+}ions of the oxide have no valence electrons to produce peaks with energy similar to those observed for the metal. Mechanism (1) invokes two-atom cross-transitions using singlet and triplet coupling, while mechanism (2) suggests three-atom cross-transitions.

4.3.1 Co-deposition of Al and oxygen (XPS)

Co-deposition of Al and O_2 yielded the 74.3 eV peak (Al 2p) for the first three deposition episodes (see sec. 3, fig. 3.5). This deposition time corresponds to aluminium oxide thicknesses in the sub-monolayer regime. This peak, as we already mentioned above, was initially observed by Flodstrom et al[114] for Al(111) and was attributed to chemisorbed oxygen. As the Al_2O_3 thickness increased (from the 4^{th} deposition episode), the 74.3 eV shifted to a binding energy value of 75.8 eV characteristic of trivalent $Al^{3+}$and reacted chemisorbed O_2 respectively. Since the deposition conditions (O_2 exposure, substrate temperature and deposition rate) were held constant, we believe that the shift was not due to changes in O_2 exposure but thickness change since this was the only variable. In fact, the shift at 40 minutes seems to correspond to the completion of the first layer as we saw in the AE intensity time plots (fig. 3.7). It should be mentioned at this point that the resolution of our spectrometer was not good enough to resolve the Al 2p emissions into its constituent $2p_{3/2}$ and $2p_{1/2}$, respectively. Thorough resolution of the Al 2p signal was additionally hampered by the presence of the Cr 3p emission around 75 eV. This was the reason why the results presented of the Al 2p region were difference spectra, i.e., each spectrum was obtained by subtracting the spectrum of Cr_2O_3 from that of the deposition run.

Previous workers have hardly mentioned the Al 2s state, which, in our case, was very important because it does not overlap with any substrate photoelectron peaks. Similar shifts (from 119.1 to 120.3 eV) in the 2s binding energies as observed for the 2p peaks after the

first three depositions were observed here, too. We make the same conclusions here that the shifts were thickness controlled rather than being caused by changes in O_2 exposure.

To investigate our thin films further, we fitted some raw data using the peak fitting program XPSPEAK4.1 by R. Kwork[84]. The experimental data for the O 1s regions of the substrate (Cr_2O_3) as well as a 13 Å thick Al_2O_3 (see fig 3.10) were considered. The same procedure was repeated for the Al 2s and 2p regions (fig. 3.11). The O 1s fits show a small but relatively significant feature at 533.5 eV for Cr_2O_3. This peak is normally identified as originating from water ligands (hydroxide and hydroxyl species). It is probably small because the crystal was annealed to 1023 K during oxidation, a situation that is believed to lead to the formation of an anhydrous oxide. The O 1s fit of Al_2O_3 on the other hand shows a relatively large H_2O contribution at 534.5 eV. This is not unexpected, as this observation has been made for Al_2O_3 even at temperatures above 1000 K (deposition at 825 K)[115]. Also, both oxides may have different affinities for H_2O species in vacuum depending on surface terminations.

Binding energy values around 530 eV are characteristic of O^{2-} anions in oxides. O 1s values for Cr_2O_3 reported in the literature range from 530.0 to 530.8 eV[116,117,118,119], whilst those for Al_2O_3 appear around 531.6 eV[118]. In this work, the O 1s peak of the O^{2-} anion for Cr_2O_3 appears at 531 eV, whilst that for Al_2O_3 is found at 532 eV. These values compare well with those reported in the literature. The Al 2p binding energy value observed for the thin Al_2O_3 films in this work occurs at 75.8 eV and agrees well with the literature. The energetic position of the Al 2s signal at 120.3 eV also suggests the Al^{3+} valence state (Fig. 3.11).

.

4.4 NMR

The structure and bonding in allyl metal compounds has been the subject of investigation since the early 60s[85]. McClellan et al[86] and Nordlander and Roberts[120] were able to show by ^{1}H-NMR as far back as 1960 that there are three types of allyl metal compounds. Allyl compounds of transition metals were known to be mainly of the π- and σ-types, whilst those of main group elements are mainly dynamic. The ^{1}H-NMR spectrum of such a system (dynamic) would yield two resonances only, a quintet and a doublet in the ratio 1:4. This would mean that the protons of the CH_2- groups cannot be distinguished from one another[85]. If, on the other hand, the allyl group is symmetrically bonded to the central metal atom, then three resonances (a multiplet and two doublets) with the intensity ratio 1:2:2 would be observed. This would suggest that the protons of the terminal CH_2- groups are distinguishable in pairs.

The ^{1}H-NMR results we obtained for the complex in d_{12}-pentane showed five resonances (500.13 MHz, pentane-*d12*, 293 K; δ) -0,20 (H'_{anti}), 2.00 (H'_{syn}), 2.93 (H_{anti}), 3.20 (H_{syn}), 4.15 (H_x). The ^{13}C-NMR spectrum shows three distinct signals with a very smooth background: ^{13}C{1H} NMR (150.87 MHz, 293 K; δ): 102 (s), 67 (s), 49 (s). We have already established the fact from our NMR data (^{1}H,^{13}C) that the terminal C- atoms of each allyl group do not interact with the metal in the same way. This would only provide one possibility of arranging the allyl units around Mo and a tetrahedral arrangement would be the most energetically favorable one.

For the first time, solid state NMR was used to investigate the complex. This was done because most solids loose their structural integrity in solution. Even though the literature sources on the positions of the ^{1}H and ^{13}C NMR resonance positions turned out to be accurate, not a single original NMR spectrum of the complex had been previously published. In most cases, this is an indication of poor spectrum quality and contaminated products. Our spectra could therefore serve as references for future work involving $Mo(C_3H_5)_4$.

4.5 XAFS

As the crystal structure of $Mo(C_3H_5)_4$ is unknown, we used the compounds $Mo(CO)(C_3H_5)_2$[1] and $Mo_2(C_3H_5)_4$[121] to calculate the reference paths for the allylic carbon atoms. In these compounds, due to symmetric π-bonding, all allylic carbons are located at approximately the same distance from the metal atom (with a deviation of max. 0.05 Å which lies within the detection limit of XAS). In addition, the crystal structures of these complexes have been elucidated and documented. By performing a thorough XAS analysis, one can distinguish between a symmetric π- and an asymmetric σ- system. In the former case, the Fourier transformed spectrum should only show one peak while in the latter, it should show two scattering contributions. To address this question, we performed three fits, namely (i) using one Mo-C shell, (ii) using two Mo-C shells with the same Debye-Waller factor and (iii) using two Mo-C shells with different DW factors. The coordination number of the second shell has been constrained to be two times the one of the first shell. Freeing the DW factors had no change on the R-factors and absolute χ^2 values. Introducing a second shell with free parameters led to a strong increase in the reduced χ^2 values. Evaluation of the different fits shows that fit (i) represents our data best. The coordination number of 3.6 shows an average presence of 3-4 allyl ligands. The distance (2.35 Å) is an acceptable value and compares well with values found in the literature for similar compounds. The fact that both C shells appear at the same distance from the absorber can be interpreted in two ways: either the compound shows a π-bonding mode with equal Mo-C distances for 1st and 2nd shell, or the structural and vibrational disorder is so high, that the average distance of the C atoms is 2.35 Å. The low CN of the first shell (3.6 instead of 4) already points at a certain degree of disorder.

The need to carry out EXAFS analysis of the Mo K-edge of the pure compound arose not only because of the excellent crystallographic data that is possible with EXAFS, but also because combined with NMR, the two methods supplement one another very well. Therefore information supplied by one method has to be replicated by the other; otherwise the need to re-check one's results becomes a necessity.

4.6 The wet chemical reactions

4.6.1. UPS

In order to understand the UP spectra fully, one should take a look at the positions of the electronic states of the allyl radical in the gaseous phase as shown in table 4.2. Table 4.2 shows a survey of theoretical and experimental results obtained for the allyl radical. The acronyms GVB and GVB-SP stand for generalised valence band and spatially generalised valence band wave function methods respectively. SCVB depicts the spin coupled valence band approach. The underlying principles behind the various *ab iinitio* methods highlighted above are beyond the scope of this work.

Table 4.2 Location of the electronic states of the allyl $(C_3H_5)^+$ radical[94,122]

State	**Type**	**Transition energies in eV**				
		GVB	**SCVB**	**GVB-SP**	**MO-CI**	**Expt.**
$X\ ^2A_2$	Valence	0	0	0	0	0
$2\ ^2A_2$	Rydberg	….	….	5.37	6.61	….
$3\ ^2A_2$	Rydberg	….	….	7.69	….	….
$4\ ^2A_2$	Rydberg	….	….	7.71	….	….
$1\ ^2B_1$	Valence	3.25	3.19	3.19	3.13	3.07
$2\ ^2B_1$	Rydberg	4.87	6.54	4.70	5.52	5.00
$3\ ^2B_1$	Rydberg	5.62	….	5.47	6.41	….
$4\ ^2B_1$	Rydberg	….	….	7.58	7.34	….
$1\ ^2B_2$	Rydberg	….	5.78	….	5.26	5.15
$2\ ^2B_2$	Rydberg	….	6.61	….	6.14	….
$1\ ^2A_1$	Rydberg	7.04	5.12	….	5.33	4.97
$2\ ^2A_1$	Rydberg	....	5.70	….	5.86	….

All electronic states are seen to occupy the region between binding energy values of 0 and 8 eV. These values compare well with the region covering the broad shoulder and the sharp peak at ~ 14 eV. Upon heating the sample, we observed a general decrease in the intensity

of the 14 eV peaks, whilst the broad shoulder was enhanced further. There was no shift in the position of both peaks, which indicates that there is no apparent change in the chemistry and consequently the electronic density of states in the temperature window investigated. We therefore conclude that the allyl species at room temperature and that at 798 K have to possess similar electronic densities of states and consequently also similar geometric structures.

4.6.2 MS

The mass spectra obtained can only easily be understood when one takes a look at the fragmentation pattern of the allyl radical. During the fragmentation of the latter, cyclopropene, allene and propyne may not be distinguishable by MS, as they all have the same molecular formula (C_3H_4). Similarly, the C_3H_3 series involving propargyl or cyclopropenyl units are possibilities. The acetylene and methyl moieties are also not uncommon[92]. A recombination of each of these units is possible making the appearance of C_4, C_5 and even C_6 units a possible likelihood. Hydrogen, either in the atomic or molecular form is also evolved.

Iwasawa et al[6] monitored the various fragments that develop after annealing $Mo(C_3H_5)_4$ impregnated on powdered alumina samples to various temperatures. The complex structure showed below was observed to fragment at high temperatures (373-870 K) to produce a wide range of fragments.

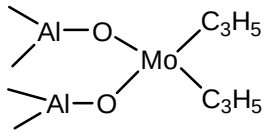

(I)

They also observed that the activity of the fixed complex (I) increased with increase in evacuation temperature before reaction. The optimum temperature of evacuation was found to be ca. 410 K. In what was assumed to be the reductive decomposition of the fixed complex, hydrogen, methane, ethane, ethylene, propane, propene, butane and butane were observed in the temperature range 373-870 K.

In the mass spectra shown in figure 3.29, we saw the onset of desorption of hydrogen, methane, ethene, propene, butene, butane and the allyl cation itself in the temperature window 598 -798 K. This presents a very similar picture to the one painted by Iwasawa et al[6] and gives credence to the fact that the wet chemical reaction between Al_2O_3 films and the allyl complex had yielded the desired results. Also, for the temperature range investigated, it would seem that the stabilities and fragmentation modes of the fixed complex in both cases compare favourably.

We also saw that with increasing temperature, there was an enhancement of the Al 2s and 2p photoelectron peaks. This trend would suggest a layer-by-layer desorption of the allyl unit. In XPS, the Mo 3d peak appears first at 648 K with a very weak intensity. We do not know at this time what the reason for this behavior and of the weak signals of molybdenum were. We know that molybdenum has a very high sensitivity factor, and must therefore appear with a relatively strong signal. The bonding scenario on the surface could have been better addressed by ARXPS (angle resolved x-ray photoelectron spectroscopy), which was impossible to carry out because of the configuration the vacuum chamber. More allyl desorption was followed by further enhancement of the Al photoelectron peaks. That mass 28 originates from ethene and not carbon monoxide or molecular nitrogen is supported by the absence of O_2, N_2 and NO at m/z 32, 28 and 30 respectively. Up to the final annealing temperature of 798 K, significant amounts of hydrocarbon (C_2H_4) and molecular hydrogen desorption were observed. Again, the C 1s region in the corresponding XP spectra further buttresses the fact that even at these high temperatures, the desorbing species still arise from hydrocarbon units on the surface and not from graphite or carbides.

.

4.7 Preliminary catalysis

The results obtained for preliminary metathesis test presented in section 3.6 can be better understood if one takes a critical look at the fragments observed in figures 3.29 and 3.31 after temperature induced desorption experiments respectively. For the sake of clarity, both figures are presented again.

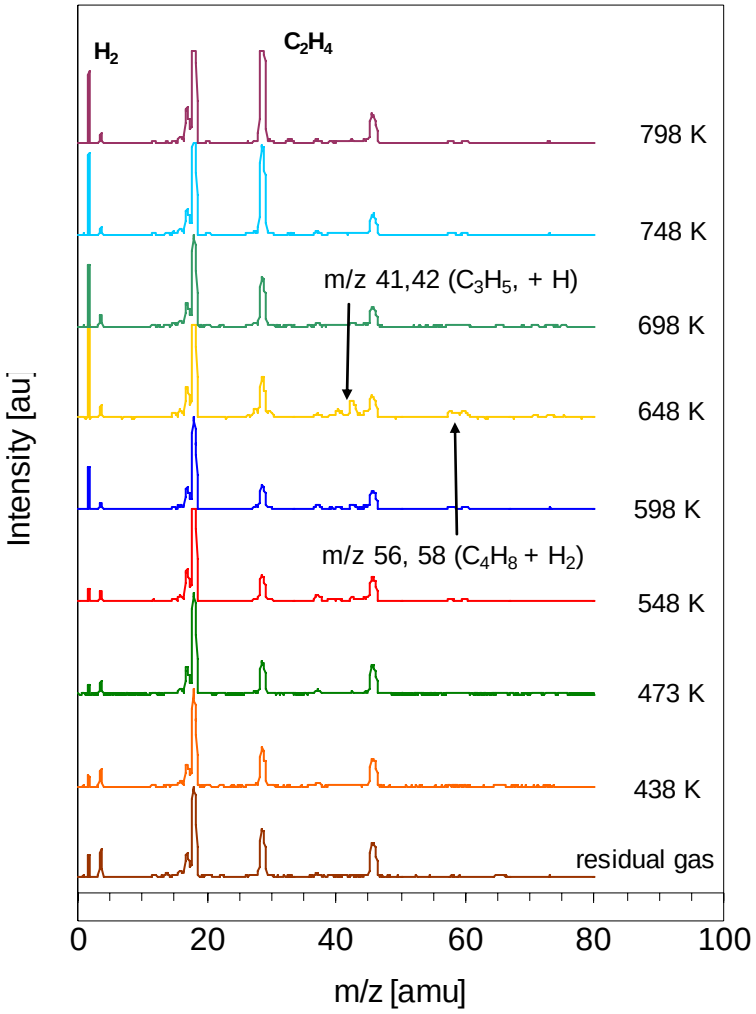

Figure 3.29: Fragmentation pattern of $(>AlO)_2Mo(C_3H_5)_2$ without propene dosage

The fragmentation pattern of the adsorbed species with temperature above is very different from the one after dosing about 3500 L of propene at 300 K. In the absence of propene, there is massive hydrogen and ethelene desorption in the 598 – 798 K temperature range. Only traces of masses 56 and 58 appear between 548 and 648 K. In fact, the spectra are completely dominated by masses 2 and 28 at high temperatures. Masses 41 and 42 also peaked off at 648 K. By contrast, however, the fragmentation pattern after propene

adsorption invokes a completely different story. Mass 28 is completely suppressed at high temperatures, whilst the 56 and 58 peaks dominate the spectra.

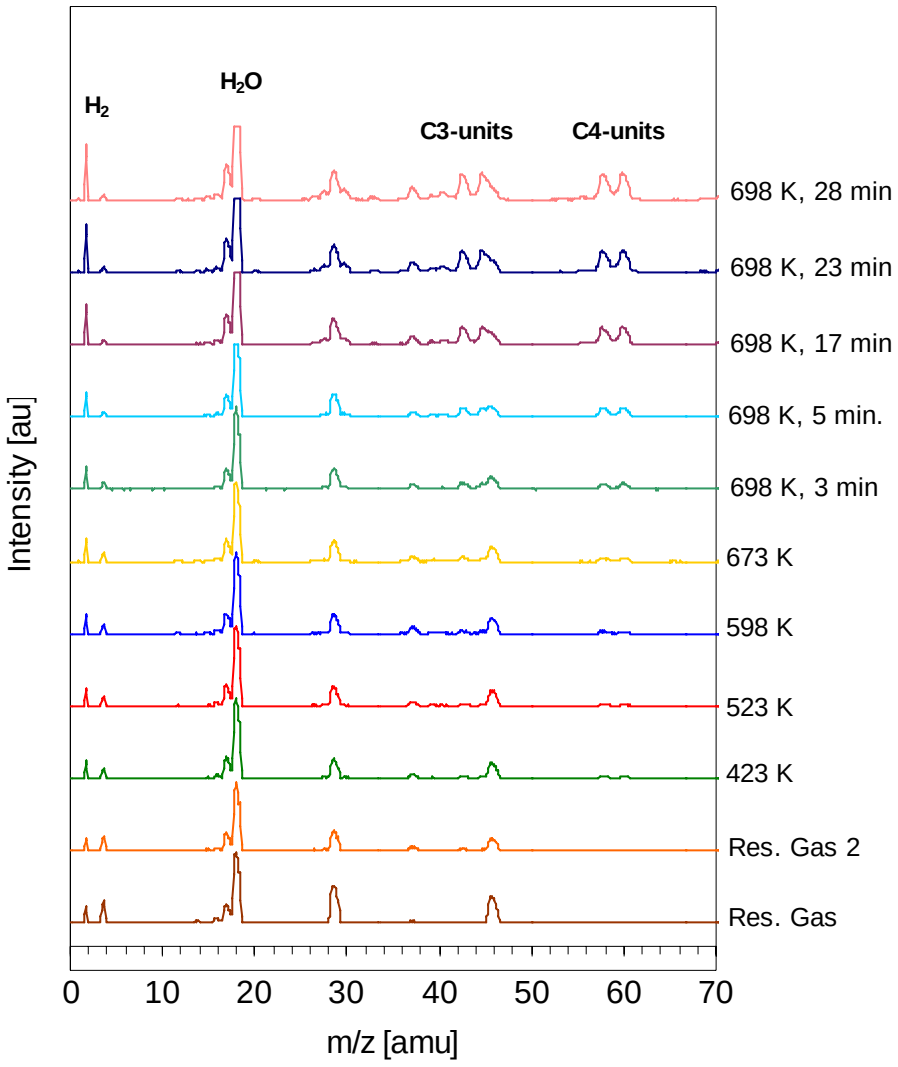

Figure 3.31: Fragmentation pattern of $(>AlO)_2Mo(C_3H_5)_2$ on exposure to 3500 L propene at 300 K.

We observed their development at 598 K and this trend continued to grow in strength until 698 K. At this temperature, even after heating for 30 minutes, there was still massive desorption of these C4-units. C3-units (allyl radical, propene, etc.) also showed up in significant amounts at this temperature. The scenario would therefore suggest that propene adsorption on the active catalyst enhances the recombination of C2 units to form the C4-units. This would explain the suppression of the intensity of ethene in favour of the butene

and butane. We can understand this behavior fully if we take a look at the observations of Iwasawa[6] and co-workers on real catalysts. Indeed they observed that if the active catalyst species is the $(>Al\text{-}O)_2Mo(C_3H_5)_2$ and the reactant is propene at 273 K, the selectivity of the reaction is 99.8% in favour of 2-butene rather than ethylene.

The observations described above are only preliminary and must be appreciated with caution for obvious reasons. First, because of its large volume and the heteromolecular nature of the residual gas environment, the analysis chamber is not a catalysis cell. Second, the observed fragmentation may have been coming from the back or the edges of the crystal rather than the surface. Third, control tests on the alumina support without the allyl complex and probably even the chromia sub-support are necessary in order to clearly map out the potentially active surface and draw useful conclusions.